

AEROELASTIC SIMULATIONS OF FLEXIBLE AIRCRAFT WITH THE COMMERCIAL STRUCTURAL SOLVER ABAQUS

Marcos C. Ruggeri¹, Roberto G. A. da Silva², Carlos E. de Souza³

¹ Technological Institute of Aeronautics (ITA)
Pça. Mal. Eduardo Gomes 50, São José dos Campos, SP, 12228-900, Brazil
mruggeri@ita.br

² Technological Institute of Aeronautics (ITA)
Pça. Mal. Eduardo Gomes 50, São José dos Campos, SP, 12228-900, Brazil
gil@ita.br

³ Federal University of Santa Maria (UFSM)
Av. Roraima 1000, Santa Maria, RS, 97105-900, Brazil
carlos.souza@ufsm.br

Keywords: aeroelasticity, simulation, flexible, aircraft, Abaqus

Abstract: The present work deals with time response and stability simulations of flexible wings using a structural commercial solver, Abaqus. The use of commercial codes for structural analyses are necessary due to their ability to deal with more complex geometry than in-house codes usually do. The problem becomes establishing strategies for coupling these codes with the different aerodynamic solvers. In aeroelasticity this coupling involves passing displacements, velocities and forces from one model to another. Here, Abaqus is coupled to the commercial aerodynamic solver ZAERO. Initially, static stresses are computed based on loads obtained from trim analyses with ZAERO aiming establishing procedures for information coupling between codes. As a first approach, a simplified cantilever rectangular plate with a concentrated mass modelling a ballast located at the wing tip is simulated and then the results are correlated to experimental data for validation. Secondly, a more complex model of an aircraft is also analysed using the same methodology as described above. Finally, some conclusions are presented regarding the importance of including nonlinearity effects in the formulation of flexible wings and then compared to the same simulations assuming a linear theory. Final comments are also mentioned with guidelines for the computational procedures and limitations on the assumptions made to get reasonably accurate results.

1 INTRODUCTION

The implementation of numerical tools in engineering often lead to codes dedicated to very limited models, either in mesh size or geometry complexity. One way of overcoming that is to use commercial softwares, that are expected to have a larger applicability, i.e., offer the possibility of modeling any kind of geometry. In addition, the solutions are usually well validated by multiple users, thus reducing the chance in errors occurrence.

Abaqus is one of the industry standards for nonlinear structural analysis, with embedded large displacements capability from its very first version. It also offers the possibility of running user subroutines in well known programming languages such as Fortran or C. All problems related with finite element modeling, data reading, finite element implementation, time integration procedures, among many others, can be left to the software, and the only problem left is the right

implementation of the user routine. In the present paper, the problem of aeroelastic simulation of flexible aircraft is addressed, focusing on the coupling of two commercial codes and a few in-house codes.

The coupling of elastic structural, aerodynamic and inertial effects on aerospace aircraft can influence seriously the integrity of the structure. This makes critical the study of aeroelastic phenomena to evaluate quantitatively the operational limits of the flight vehicles in order to comply with design and certification requisites. Aeroelastic interactions are important since they determine airplane loads and can influence flight performance in several areas such as aerodynamic lift redistribution, stability derivatives (including lift effectiveness), control effectiveness (including aileron reversal), structural static and dynamic stability (divergence and flutter) and aircraft structural dynamic response to turbulence and buffeting, among others.

The first topic is relevant since this effect modifies lift loads on the wing and tail surfaces due to change in external preliminary loads computed as rigid. In second place, the stability derivatives may impact on the flight static and dynamic control such as trimming of the aircraft and dynamic response. The next issue is related to the loss of response of the control surfaces due to excessive torsion of the airfoil section induced by structural deformations reducing the effective angle of attack, which can be limit considerably the maneuverability of the aircraft. In addition, lack of static and dynamic stability also plays an important role in the aeroelastic phenomenon, where a correct understanding of the physics must be taken into account to avoid potential issues, or even worse, catastrophic failure. Finally, the atmospheric influence of gusts and turbulence over the air free-stream can change the effective incidence of the aerodynamic surfaces, so causing sudden changes in the lift forces and hence dynamic response of the aircraft involving flexible deformations, specially large ones for slender structures.

In this work only the last three phenomena mentioned above will be analyzed for different case studies. The first one is a simple slender plate modeling a rectangular wing with a ballast located at the wing tip. Studies of trimming are first performed for assumed 1g non-accelerated level flight and a comparison of the rigid and flexible body is analyzed. Secondly an examination of flutter instability is done for different configurations of the offset positions of the ballast. Numerical and experimental results are then presented for the stability analysis of flutter. Extraction of the natural frequencies, real eigenvalues and mode shapes as well as modal generalized matrices are performed in Abaqus with the *FREQUENCY solver procedure. Then, a `tozaero` translator is invoked to transform the global element matrices into a universal file and finally, the flutter analysis is executed in ZAERO after importing the FEM output data previously converted. Results are then compared to experimental tests performed in the ITA/Lab. Prof. Kwei Lien Feng wind tunnel for final correlation of both methods. Some conclusions are extracted based on the obtained results.

The second problem in study will be a generic commuter aircraft. The representative model is broadly simplified in order to show only the computational methodology of the approach of flexible aircraft with commercial software. The same FEM-aerodynamic coupling procedure as described earlier is applied in this case. Some conclusions are remarked on and limitations of this procedure are also commented at the end of the work.

Lastly, some remarks are also outlined for flexible spacecraft and the spinning influence on the aeroelastic instability with the addition of gyroscopic damping terms.

2 THEORETICAL BACKGROUND

The aeroelastic processes here discussed are basically static trim, dynamic instability and a simplified time-marching solution. The formulations considered for each case are briefly discussed in the next sections.

2.1 Static aeroelastic trim formulation

Based on the well-known rigid body equations of motion, the flexibility of the aircraft now introduces a new contribution to the distributed aerodynamic and inertial forces to account for elastic deformation of the structure. For the aerodynamic forces, the flexible part is related to the structural deformation through the aerodynamic influence coefficients matrix (AIC) in the following manner:

$$\{\mathbf{F}_{\text{ar}}\} = q_\infty [\mathbf{G}]^T [\mathbf{AIC}] [\mathbf{G}] \{\mathbf{x}\} = q_\infty [\overline{\mathbf{AIC}}] \{\mathbf{x}\} \quad (1)$$

The rigid aerodynamic forces can be expressed as a function of the trim variables such as:

$$\{\mathbf{F}_{\text{ar}}\} = \{F_R(\alpha, \beta, p, q, r, \delta_i, \dots)\} = [\mathbf{G}]^T \left[\frac{\partial \mathbf{f}_a}{\partial \mathbf{a}} \right] \{\mathbf{a}\} = \left[\frac{\partial \overline{\mathbf{f}}_a}{\partial \mathbf{a}} \right] \{\mathbf{a}\} \quad (2)$$

being $\{\mathbf{a}\}^T = [\alpha \ \beta \ p \ \dots]$ the trim variables vector. Hence, the computation of the distributed flight loads of a flexible aircraft can be performed by equalling the internal forces, rigid inertial forces, rigid aerodynamic forces and incremental flexible aerodynamic forces, as follow:

$$[\mathbf{K}_{\text{gg}}] \{\mathbf{x}\} + [\mathbf{M}_{\text{gg}}] [\phi_r] \{\ddot{\mathbf{u}}_r\} - q_\infty [\overline{\mathbf{AIC}}] \{\mathbf{x}\} = \left[\frac{\partial \overline{\mathbf{f}}_a}{\partial \mathbf{a}} \right] \{\mathbf{a}\} \quad (3)$$

where the flexible inertial forces due to accelerations of structural deformation (flexible aircraft) are not considered in this case provided that they belong to the dynamic loads problem.

There are two standard formulations for solving the Equation (3), one based on the direct method (exact approach) and another that transforms the domain into the modal space. The latter formulation will be discussed here since it corresponds to that used by the commercial code ZAERO [1]. Transforming the Equation (3) to the modal space, and making use of the orthogonality properties between the rigid and elastic modes with respect to the stiffness and mass matrices, after algebraic manipulation it becomes:

$$[\mathbf{M}_{\text{rr}}] \{\ddot{\mathbf{u}}_r\} = [\phi_r]^T \left(\left[\frac{\partial \overline{\mathbf{f}}_a}{\partial \mathbf{a}} \right] + \left[\frac{\partial \overline{\mathbf{f}}_{\text{ae}}}{\partial \mathbf{a}} \right] \right) \{\mathbf{a}\} = ([\mathbf{S}_R] + [\mathbf{S}_e]) \{\mathbf{a}\} \quad (4)$$

For a given flight maneuver condition, there will be a set of known accelerations of trim degrees of freedom \ddot{u}_{r_g} and known trim variables a_g , given as input. The correspondent set of unknown trim degrees of freedom \ddot{u}_{r_u} and unknown trim variables a_u are then obtained by solving the trim analysis. After re-arranging Equation (4), it can be partitioned to separate given and unknown variables in the following fashion:

$$[[\mathbf{M}_{\text{rr}}]_u, [-([\mathbf{S}_R] + [\mathbf{S}_e])]_u] \begin{Bmatrix} \ddot{u}_{r_u} \\ a_u \end{Bmatrix} = [-[\mathbf{M}_{\text{rr}}]_g, [([\mathbf{S}_R] + [\mathbf{S}_e])]_g] \begin{Bmatrix} \ddot{u}_{r_g} \\ a_g \end{Bmatrix} \quad (5)$$

For the particular case in which the number of unknown trim degree of freedom plus the unknown trim variables equals the number of trim equations, the systems becomes determined and invertible, finally obtaining the trim variables and accelerations for the aeroelastic static equilibrium.

2.2 Dynamic instability formulation

Flutter is usually considered a self-excited phenomenon due to the coupling of two or more elastic vibration modes, leading to a dynamic instability of divergent behavior in which the air stream adds energy to the system instead of extract, situation that may exceed the operational limits of the aircraft with serious risks to the integrity of the structure.

The motion of an aeroelastic general system can be formulated in the following manner:

$$[\mathbf{M}]\{\ddot{\mathbf{u}}(t)\} + [\mathbf{K}]\{\mathbf{u}(t)\} = \{\mathbf{L}_e(t)\} + \{\mathbf{L}_a(\mathbf{u}(t), \dot{\mathbf{u}}(t))\} \quad (6)$$

The right hand side of Equation (6) represents the aerodynamic load, which is decomposed into two separate contributions, one related to external forces $\{\mathbf{L}_e(t)\}$ (e.g. gust, external effects from control systems, ASE) and other contribution coming from the incremental loads dependent on the displacements $\{\mathbf{L}_a(\mathbf{u}(t), \dot{\mathbf{u}}(t))\}$, whose value can be obtained from the non-stationary aerodynamic theory.

In order to study the flutter phenomenon it is necessary to formulate properly this aerodynamic loading as a function of displacements, velocities and even accelerations of the structure. The inclusion of a non-stationary aerodynamic model is needed to effectively capture the vorticity effect present on the downstream wake, which in turn creates aerodynamic lag linked to the loads induced by the deformations. The general model of Theodorsen [3] is able to formulate this by splitting the aerodynamic loads into two contributions, named as *non-circulatory terms* and *circulatory terms*. The former considers the air flow is expressed as elemental fonts and sinks singularities, where the latter represents the wake vorticity from the trailing edge downstream towards the infinity and depends on the known Theodorsen complex function $C(k) = F(k) + iG(k)$. This function can be interpreted as the lift deficiency that modifies the circulation over the airfoil by the influence of the normal downwash (Q).

Assuming that the flutter condition is taking place at a neutral stability state associated to a simple harmonic motion, this type of motion was chosen to represent the oscillatory motion of the wake in terms of reduced frequencies. In the neutral aeroelastic stability condition, the indifferent equilibrium must be satisfied whatever be the deformed position. Thus, the external loads $\{\mathbf{L}_e(t)\}$ can be canceled on Equation (6), leaving only the incremental aerodynamic loads:

$$[\mathbf{M}]\{\ddot{\mathbf{u}}(t)\} + [\mathbf{K}]\{\mathbf{u}(t)\} - \{\mathbf{L}_a(\mathbf{u}(t), \dot{\mathbf{u}}(t))\} = \{\mathbf{0}\} \quad (7)$$

It is convenient to transform Equation (8) into the Laplace frequency domain, where the aerodynamic load can be considered as output due to the deformation states together with its derivatives. Representing this aerodynamic load as a Duhamel integral, the indicial response of the system will be expressed as the aerodynamic transfer function $\bar{H}(sb/V_\infty)$ in terms of the adimensional Laplace variable. The system is now an eigenvalue problem in the Laplace domain:

$$\left(s^2[\mathbf{M}] + [\mathbf{K}] - q_\infty \left[\bar{\mathbf{H}} \left(\frac{sb}{V_\infty} \right) \right] \right) \{\mathbf{u}(s)\} = \{\mathbf{0}\} \quad (8)$$

The aerodynamic loads term has been computed historically by two methods. The first one was associated to the extension of the bi-dimensional flutter theory (typical section of Theodorsen) to the three-dimensional effects through the Strip Theory [3] for the case of high aspect ratio unswept wings. Barmby (NACA-TR-1014) and Yates (NACA-RM-157) later extended this method to the Modified Strip Theory that takes into account general swept wings with compressibility corrections. Nevertheless, a more recent theory developed in the last decades is associated to the three-dimensional aerodynamic theory through the discrete element methods, also known as panel methods. Here it will be only formulated the latter, since it is that one used in the ZONA6 method developed by ZONA Technology. This method is based on the known Kernel functions for the computation of the aerodynamic loading. Based on the linearized perturbation velocity potential equation:

$$(1 - M_\infty^2)\tilde{\phi}_{xx} + \tilde{\phi}_{yy} + \tilde{\phi}_{zz} - 2\frac{M_\infty^2}{V_\infty}\tilde{\phi}_{xt} - \frac{M_\infty^2}{V_\infty}\tilde{\phi}_{tt} = 0 \quad (9)$$

Assuming that the perturbation potential varies harmonically given by the relation $\tilde{\phi}(x, y, z, t) = \tilde{\varphi}(x, y, z, t)e^{ikt}$, Equation (9) can be transformed into the reduced frequency domain. The discrete element method consists in subdividing the domain into discretized regions and collocating distributions of flow singularities (which elementary solution is known) and then applying the superposition principle as a sum of solutions. For a general body distributions of fonts and dipoles should be collocated on the surface and dipoles downstream to model the wake. However, considering a body as lifting surface located on the x-y plane (with no thickness), it will be only needed to use dipoles distributions, provided that fonts are only required for modeling bodies with finite thickness.

The effect of the wake has as finality to keep memory of the aerodynamic lag induced by the vortex wake of the lifting surface. In this way, for a approach with good precision the wake should be modeled from the trailing edge down to a far distant region. This leads as disadvantage a high computational cost required. To overcome this issue, it is more convenient to use the perturbation acceleration potential instead. Since there is no pressure jump associated when crossing the trailing wake, now only the wing domain will be necessary to be modeled.

Imposing the normal downwash at the 3/4 chord position, the problem is now in the closed-form with pressure values as unknowns. The incremental aerodynamic loading given in Equation (6) gets the following fashion expressed on the aerodynamic grid reference:

$$\{\mathbf{L}_a(ik)\}_{\text{aero}} = q_\infty[\mathbf{S}][\mathbf{AIC}(ik)][\mathbf{F}(ik)]\{\mathbf{h}\} \quad (10)$$

For those cases in which the structural grid differs from the aerodynamic grid, a technique for interpolating nodal displacements (structural domain) is needed to get the displacements at the 3/4 chord control points (aerodynamic domain). An interpolation splines matrix is then defined to transform the mode shapes transformed from one domain to other. The aerodynamic loading on Equation (10) can also be transformed into the aerodynamic grid through the virtual work principle, assuming the virtual work of these loads be the same regardless what referential is used. After algebraic manipulation it becomes:

$$\{\mathbf{L}_a(ik)\}_{\text{struc}} = [\mathbf{G}]^T q_\infty[\mathbf{S}][\mathbf{AIC}(ik)][\mathbf{F}(ik)][\mathbf{G}]\{\mathbf{u}\} \quad (11)$$

Due to the fact of having the finite element model a number of degrees of freedom excessively

high, it is appropriate to further transform the domain into the a modal basis, greatly reducing the size of the problem to a few modal degrees of freedom depending on the amount of selected elastic modes. Also, taking advantage of the orthogonality properties of natural modes with respect to the mass and stiffness matrices, the generalized matrices will be diagonal and uncoupled, unlike the aerodynamic load that will be in general fully coupled. The full aeroelastic system in the modal base will then be:

$$(-\omega^2[\bar{\mathbf{M}}] + [\bar{\mathbf{K}}] - q_\infty[\bar{\mathbf{Q}}(ik)]\{\mathbf{q}(i\omega)\}) = \{\mathbf{0}\} \quad (12)$$

Several methods are currently available for the calculation of the aeroelastic system. One of them is the k-method, which consists in adding an artificial damping required to destabilize the system and ensure that the simple harmonic motion as proposed by Theodorsen. This artificial damping strictly has no physical meaning, except on the flutter condition, but is a technique used to compose the V-g curves. The aeroelastic equation to be solved by the k-method with the addition of artificial damping will be finally:

$$(-\omega^2[\bar{\mathbf{M}}] + (1 + ig)[\bar{\mathbf{K}}] - q_\infty[\bar{\mathbf{Q}}(ik)]\{\mathbf{q}(i\omega)\}) = \{\mathbf{0}\} \quad (13)$$

Another well known technique for solving Equation (12) is the g-method [5], considered as a k-method evolution. The g-method was created in order to correct some possible inconsistencies that may exist in the former k-method and make results more reliable by using a first-order damping perturbation in the flutter equation and transforming it into state-space form. Unlike the k-method, the procedure now solves for real, not artificial damping.

2.3 Time response formulation

The time response can be obtained directly by time integration of the structural equations of motion. Blair et al. [11] presented aeroelastic time domain simulations where Equation (6) is rearranged, taking the constant components of the aerodynamic loading to the left side of the equation. The mass and stiffness matrices were computed a priori by a Finite Element solver and the solution is marched in time using Newmark method.

In the present case, however, the goal is to investigate the use of the Abaqus time integration routines and only implement the aerodynamic loading. Abaqus allows the definition of user routines for implementation of distributed loads at each time increment. The right side of equation (6) can be adapted for implementation in the user subroutine:

$$\{F_e(t)\} = \{L_e(t)\} + \{L_a(\mathbf{u}(t), \dot{\mathbf{u}}(t))\} \quad (14)$$

Abaqus offers two approaches for dynamic and nonlinear problems: the implicit scheme, using Hilber-Hughes-Taylor time integration, and the explicit scheme, using a central-difference operator [2]. There is a user routine available for each case: the `DLOAD` for the implicit scheme and the `VDLOAD` for the explicit.

3 NUMERICAL IMPLEMENTATION

Figure 1 shows a schematic visualization of the work flow for aeroelastic simulations with commercial softwares Abaqus and ZAERO. It consists on first running an eigenvalue procedure on Abaqus to extract the natural frequencies and mode shapes. Secondly, a `tozaero` translator

interface is invoked to transform the output global element matrices into an universal file to be read by the aeroelastic code. A trim analysis is then simulated with ZAERO to couple the aerodynamic loading and calculate the lift distribution on the flexible body, inducing in turn associated structural deformations. The `PLTTRIM` bulk data card is used to generate the plot files of the deformed aerodynamic model and steady pressure distributions, and to generate a file that contains the flight loads in terms of concentrated forces and moments bulk data cards at the structural finite element grid points. The ZAERO aerodynamic results are finally coupled back into the finite element model in Abaqus to perform a static analysis for detailed stress calculations of the flexibly structure. As shown on the flowchart, a flutter analysis can also be done and the `PLTFLUT` bulk data card is invoked to generate the post-processing results for flutter modes. The reader should note that the file extension of the ZAERO input deck was changed to `.INPZ` in order to avoid confusion with the Abaqus input file.

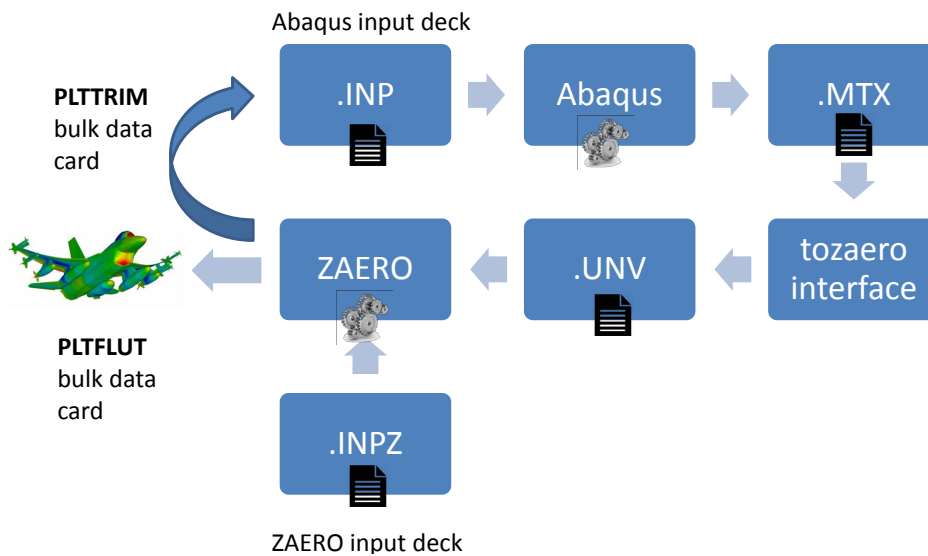


Figure 1: Flowchart for the coupling process between Abaqus and ZAERO software.

On the other hand, for correlation of the numerical results an in-house vortex lattice code was implemented on MATLAB for the wing case study. The code up to now is only limited to non-twist planar wings (no dihedral) with symmetric flow, but it is expected that currently ongoing developments will extend this functionality. The rigid body case is first considered for the aeroelastic trim analysis and only the right half-wing is modeled, but taking into account the aerodynamic influence of the left half-wing on the AIC matrix construction. To avoid the tendency of the VLM to predict low values of induced drag, corrections of the induced drag spanwise distribution are made on the in-house code by introducing a correcting scale factor into based on the cross-flow energy in the wake following Kalman et al. [8]. As usual, the boundary condition is imposed on the control point of each aerodynamic panel to guarantee the tangent air flow condition to finally get the closed-form problem with vortex singularities as unknowns.

The time marching solution is being implemented in Abaqus by means of the the user subroutines `DLOAD` and `VDLOAD`. For implementation of aerodynamic loading, the explicit routine offers one advantage: it allows access to the velocity at the points where the load is to be computed. The implicit scheme would require that the user routine accessed a temporary file to save the instantaneous position at the end of each increment and recovered it in the beginning of the next for computation of velocities.

4 CASES STUDIES

As a first approach, a metallic wing of aluminum material 2024 T3 is studied following the wing model B from Westin et al. [6] [7]. It is built on a plate-shaped with 0.032" thickness, and dimensions 0.35 x 0.04 m. This wing is clamped on one end to a steel mast, which consists of a tube of 1-3/4" and 1-1/4" outer and inner diameters respectively, through a support that secures it through clamping screws. The clamping of the tube is made through a steel plate welded on the lower end, whose role is to serve as a flange to be bolted on an inertial base. A concentrated brass ballast located at the free wing tip is made in such a way that it can run along the wing tip chord. The ballast center of mass is first centered at half chord position, and later sensibility studies are performed varying position of the ballast running chordwise at the free wing tip.

Firstly, the problem is addressed numerically with an Abaqus finite element model to run the natural frequencies extraction with the Lanczos eigensolver. Next, the eigenvalue solution is coupled to the aeroelastic code for the computation of the generalized aerodynamic forces contribution. The commercial code ZAERO is used in this case, being a high fidelity computational tool which allows robust non-stationary aerodynamic modeling and implementation of the k- and g-method for flutter solution, as well as other functionalities such as static aeroelastic trimming, flight loads computations, gusts, aeroservoelasticity, among others. Both static trim configuration at 1g level flight and flutter investigation are addressed for this case study.

Figure 2 shows the structural FEM model in Abaqus, meshed with S4R reduced-integration general-purpose shell elements. The mesh size is 180 elements and 217 nodes. For the cases of different ballast mass offsets a rigid beam-like CONN3D2 connector was used to link the wing tip node with the elastic axis located at the center of the mid-chord.

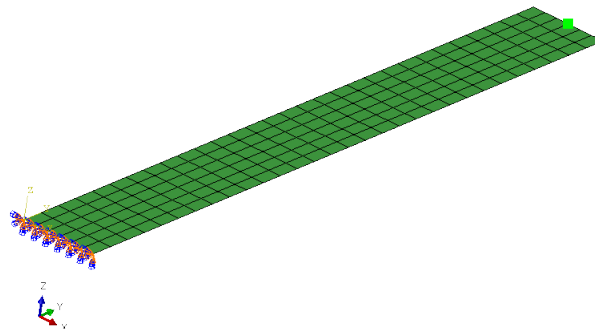


Figure 2: Structural FEM model of the rectangular rectangular plate-like wing.

Regarding the aerodynamic model, a coarser mesh was used with 40 (4 x 10) aerodynamic boxes composed by 5 divisions chordwise and 11 spanwise, as shown in Figure 3. Based on this fact, a convergence sensibility should be performed to guarantee that the aerodynamic mesh accurately capture the actual aerodynamic loading distribution, specially in those areas where there may exist large gradients such as at the wing tip. In addition, at high values of reduced frequencies this might affect the convergence of the AIC computations for large models, which in turn leads to high computational costs. As a general rule of thumb, for this kind of models it is recommended to have at least 20-30 chordwise divisions on lifting surfaces such as wing.

ZONA6 method was selected for the aeroelastic analysis and the wing is modeled as a single *macroscopic* element, defined by its root and tip leading edge coordinates respectively. On the same fashion were defined the trailing edge coordinates. The numeration sequence of the macroelement is displayed in Figure 3.

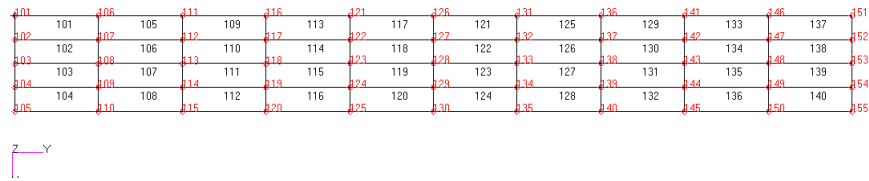


Figure 3: Aerodynamic model of the rectangular rectangular plate-like wing.

For the trim analysis, it was chosen a ballast offset configuration of 5mm positive (aftward) provided that negative offset values of the ballast position had revealed low critical flutter speeds, thus invalidating any static trim study after the dynamic instability phenomenon. An ISA atmosphere at sea level is considered in all cases, with a freestream air velocity of 10 m/s and 1g level flight condition. Symmetric air flow is considered at steady state with no slipping.

As mentioned before, the in-house VLM code is also used for this case study to simulate the trim condition at 1g level flight for the rigid and thus validate the results obtained from the ZAERO output. The model consists on 40 aerodynamic boxes with only the right semi-wing represented. The same geometry of the AE-249 straight wing is used here for results correlation: AR=17.5, no taper ratio, planar wing with no dihedral and no twist. Figure 4 shows the model with the position of the control points and quarter-chord bound vortices lines on each aerodynamic box.

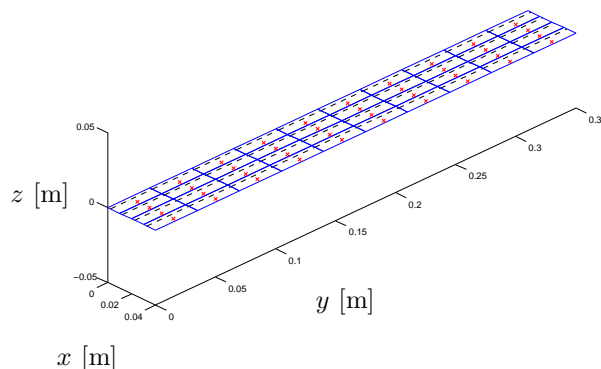


Figure 4: Aerodynamic model of right half-wing on in-house VLM code (Present).

A second chosen case study is based on a model of twin-turboprop generic commuter aircraft, as shown in Figure 5. Its geometrical dimensions are given by 15.16m overall length, 17.28m wingspan and 4.57m tailspan. The wing planform configuration consists on an unswept tapered wing with AR=10.5 and 7 degrees of dihedral angle. T-tail aircraft configurations are particularly interesting for aeroelastic coalescence of the wing-tail anti-symmetrical torsion bending mode of flutter, and its influence on the flutter speed has been studied in detail by Foltran [9]. In this model the CAD representation only considers the geometry for the external skin, engine nacelles, and some structural internal members such as bulkheads, spars and ribs of the lifting surfaces (wing, horizontal and vertical stabilizers). Concentrated masses are distributed along the aircraft longitudinal axis to represent the mass contributions of the aircraft systems and components. The aim of the study here is simply to replicate the same analysis procedure as done with the plate-like rectangular wing AE-249 to evaluate the numerical results of the aeroelastic trim condition and flutter dynamic instability for more general aircraft configurations. No experimental data is validated at this stage.

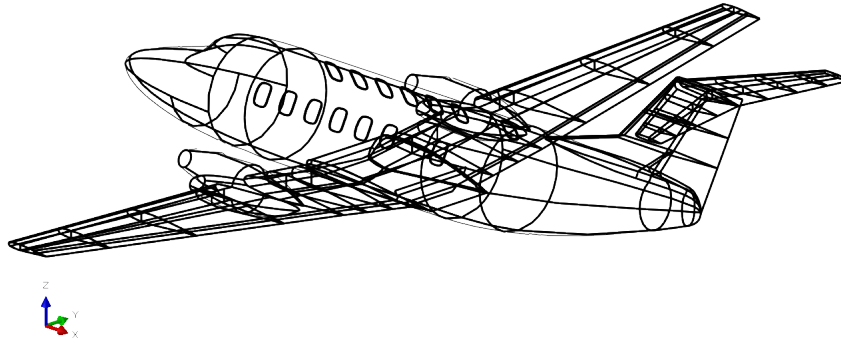


Figure 5: CAD model of the generic commuter aircraft case study.

5 RESULTS

For the first case study of the rectangular plate-like wing, on Table 1 are shown the results obtained from the eigenvalues extraction solution using the Lanczos eigensolver. The first 8 elastic modes computed on Abaqus were also correlated with output values run on MSC.Nastran using the Modified Givens solver. The relative error for each mode comparing both methods and solvers shows a very good agreement of results, indicating the second in-plane bending mode as the most critical discrepancy. This issue can be attributed to the difference of normal drilling stiffness on each formulation of Abaqus/S4R and Nastran/CQUAD4 elements. On the latter case, the drilling stiffness was calibrated using the `PARAM, K6ROT` bulk data card.

On the other hand, the effect of considering the ballast offset located 5mm aftwards from the elastic axis created a mass unbalancing at the wing tip that coupled bending torsion vibration modes at the 2nd eigenvalue, thus suppressing a pure 2nd bending mode at low frequency.

Mode	Description	Abaqus [Hz]	MSC.Nastran [Hz]	Error (%)
#1	1st bending	2.297	2.296	-0.01
#2	1st bend-torsion	23.910	24.110	+0.83
#3	2nd bend-torsion	25.434	25.632	+0.77
#4	2nd bending	78.190	77.653	-0.69
#5	1st in-plane bend.	107.410	107.341	-0.06
#6	2nd in-plane bend.	120.470	117.604	-2.44
#7	3rd bend-torsion	161.530	160.630	-0.56
#8	3rd bending	163.130	165.183	+1.24

Table 1: Comparison of first 8 free vibration modes for the plate-like wing - case 5mm pos.

The output of the aeroelastic trim analysis at non-accelerated 1g level flight are shown in Figure 6, where the deformed configuration of the wing is displayed together with the aerodynamic lift distribution over the surface in terms of concentrated forces and moments passed from the ZAERO results. By physical inspection good correlation was found after the experimental tests performed at the ITA/Lab. Prof. Kwei Lien Feng wind tunnel prior to the appearance of the flutter phenomenon.

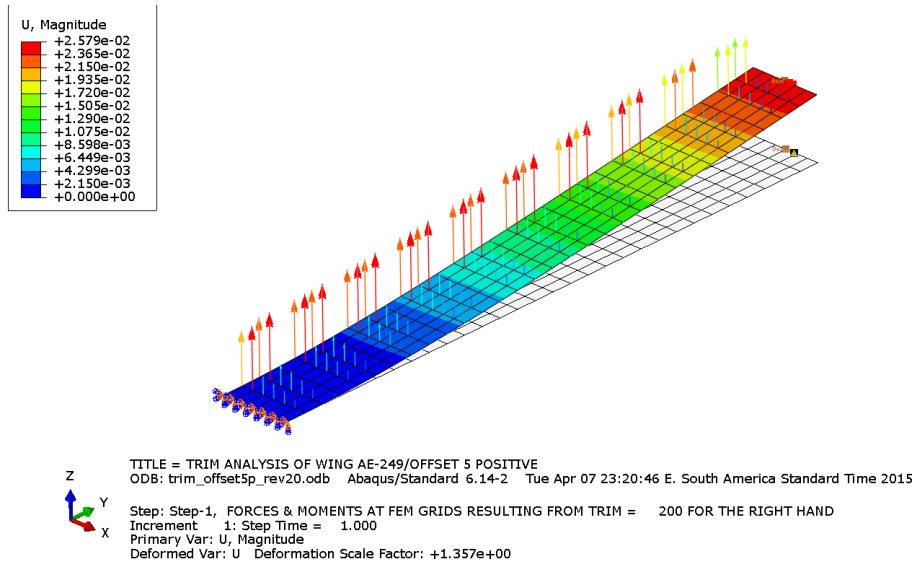


Figure 6: Deformation on flight loads at 1g level flight condition.

As mentioned on the Section 3 of this work, the same problem at 1g level flight condition for the rigid case was simulated using an in-house VLM code in order to compare the output of aerodynamic characteristics at the trimming condition. The reference AOA of 7.90194 degrees was selected based on the ZAERO rigid case for trimming, as shown in Table 2. The results of pressure coefficient distribution are displayed in Figure 7 for the right half-wing due to the assumed XZ symmetry. As can be seen, the influence of the aerodynamic mesh near the tip region is important to effectively capture the gradient of pressure distribution. Similar results were also obtained with Tornado code for this case study.

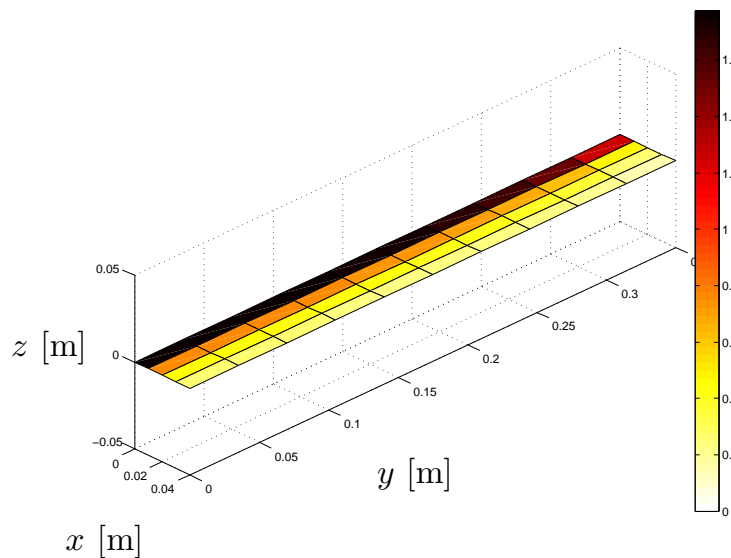


Figure 7: CP distribution results from in-house VLM code (Present) - rigid case.

The distribution of the lift coefficient along the span is shown in Figure 8, together with results obtained from the lifting line theory and bidimensional airfoil theory (flat plate). The lift distribution agreement between VLM and LLT correlates very well, even on the region near to the wing tip.

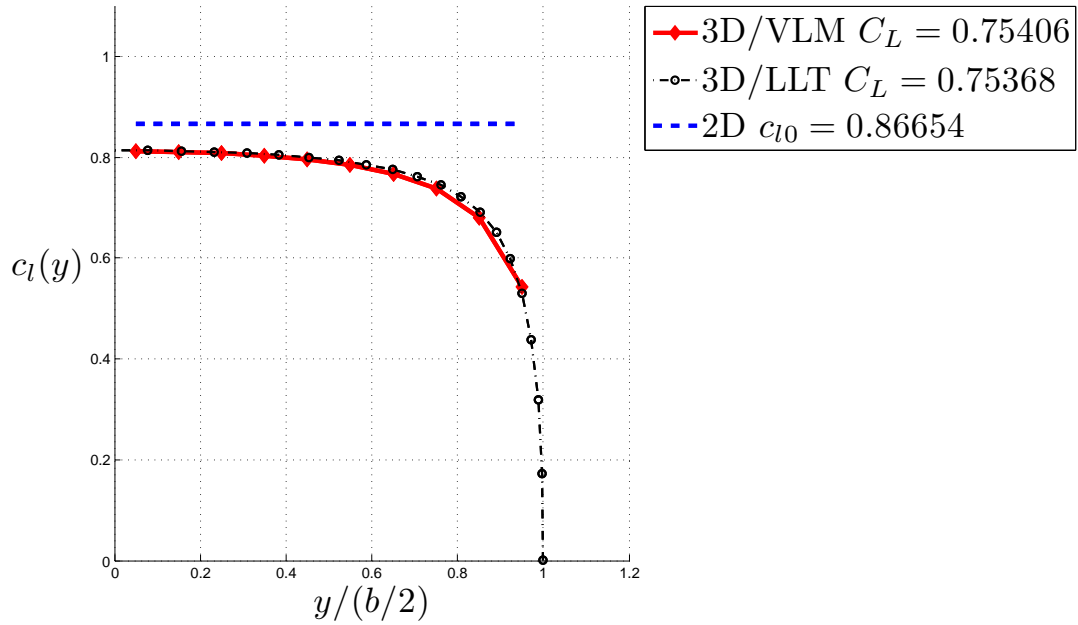


Figure 8: CL distribution results from in-house VLM code (Present) - rigid case.

On the other hand, it can be seen in Figure 9 some discrepancy on the effective AOA at stations from the 0.85 semi-span up to the wing-tip. Even though more aerodynamic boxes in the near-tip region should be used for better correlation, it was fixed on 40 panels for comparison with ZAERO at the same mesh size. The near-root region showed excellent agreement in both cases.

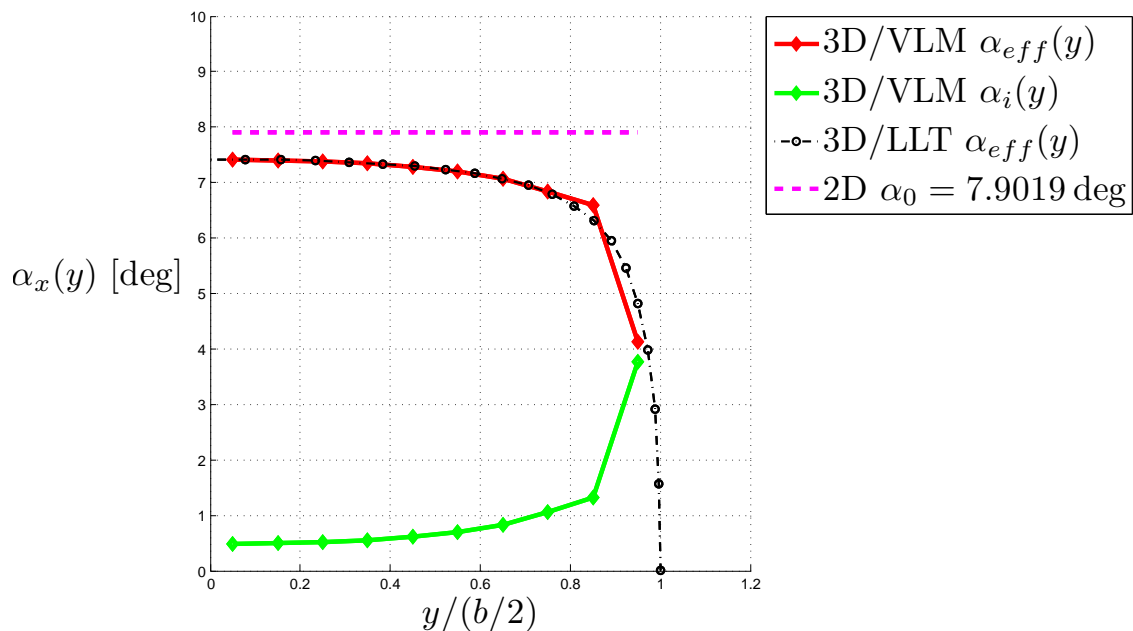


Figure 9: AOA distribution results from in-house VLM code (Present) - rigid case.

Having as reference the the trimming condition computed by ZAERO for the rigid case, Table 2 shows the results comparison for all the methods implemented. The overall error of the global lift coefficient at level flight was less than 1%, even with a coarse mesh of 40 aero boxes,

which indicates the robustness of the trimming formulation at very low computational costs. In addition, for the flexible case ZAERO showed a reduction of the approximately 3% of the global angle of attack compared to the rigid body case. It is expected that for more severe loading configurations the flexibility influence plays a more important role on the AOA variation for trimming.

In Table 2 the reader should note the difference in nearly ten times of the induced drag coefficient values calculated by ZAERO and the other codes. In the former case, ZAERO computes differently the CDi by simply multiplying $CL \sin(AoA)$ in an approximate fashion. The latter cases compute the CDi based on the downwash distribution, specifically the in-house VLM code following Kalman et al. [8].

	Semi-span	Semi-span	Semi-span	Full-span	Full-span
	ZAERO - Rigid	ZAERO - Flexible	VLM (Present)	Tornado	LLT
	40 aero boxes	40 aero boxes	40 aero panels	80 aero panels	41 stations
AoA [deg]	7.90194	7.64288	7.90194	7.90194	7.90194
CL	0.76012	0.76012	0.75406	0.75034	0.75368
CDi	0.10509	0.10395	0.011913	0.010505	0.011829
L [N]	1.3036	1.3036	1.2932	1.2868	1.2926
nz	1.0	1.0	0.99203	0.98711	0.99153

Table 2: Comparison of numerical results on aerodynamic characteristics - case 5mm pos.

With respect to the dynamic instability studies, for the 5mm negative ballast offset configuration flutter analyses were simulated on ZAERO/ZONA6 method based on the respective natural frequencies previously extracted. The decision to choose the this offset case as reference was due to the fact of having the lowest critical flutter speed for comparison with experimental data obtained in the ITA/Lab. Prof. Kwei Lien Feng wind tunnel. As shown on V-g-f curves in Figure 10, the results provided the coalescence of the modes 2 and 3 (first two bending-torsion modes) as flutter mechanism, as expected, provided that the frequencies are very close to each other to quickly promote coupling of these modes. Artificial damping of mode 3 became positive at the crossing x-axis point of 10.02 m/s defining the flutter speed.

A parametric investigation was done in order to determine the direct influence of the ballast offset position on the flutter speed. Hence, selected test cases were with 0mm, ± 1 mm, ± 5 mm, ± 10 mm and ± 15 mm offset positions. For the first configuration (offset 0mm) no flutter condition was observed, but on the remaining cases (-10mm and -15mm offset) again mode 3 became unstable. However, now the flutter speed was increased with respect to the previous cases, since as the center of gravity got closer to the leading edge the dynamic stability increased considerably. Charts in Figure 11 show the correlation of results with experimental data, after simulating with Abaqus and also comparing with MSC.Nastran.

It can be observed good overall agreement between experimental and numerical results for large negative offsets, with slight discrepancies in magnitude as offset positions were lowering. For the case of lowest flutter (1mm negative offset), strong differences between Abaqus and MSC.Nastran indicate that further investigations should be performed in order to evaluate the lack of reliability of the results. It is important to remark that there can be uncertainties

associated when estimating the actual structural damping of the wing. As a first approach all simulations did not considered structural damping, but later an arbitrary value of 1% was assumed to be constant throughout the frequency range. More rigorous modeling would require better calibration of this value. As for -10mm and -15mm offset cases, the flutter speed estimated in wind tunnel test were lower in both cases, probably associated to uncertainties at the time of observation of the test and errors in measuring instrument calibration (Betz manometer, measuring the frequency instrument) which might also induce mild inherent errors to the experiment.

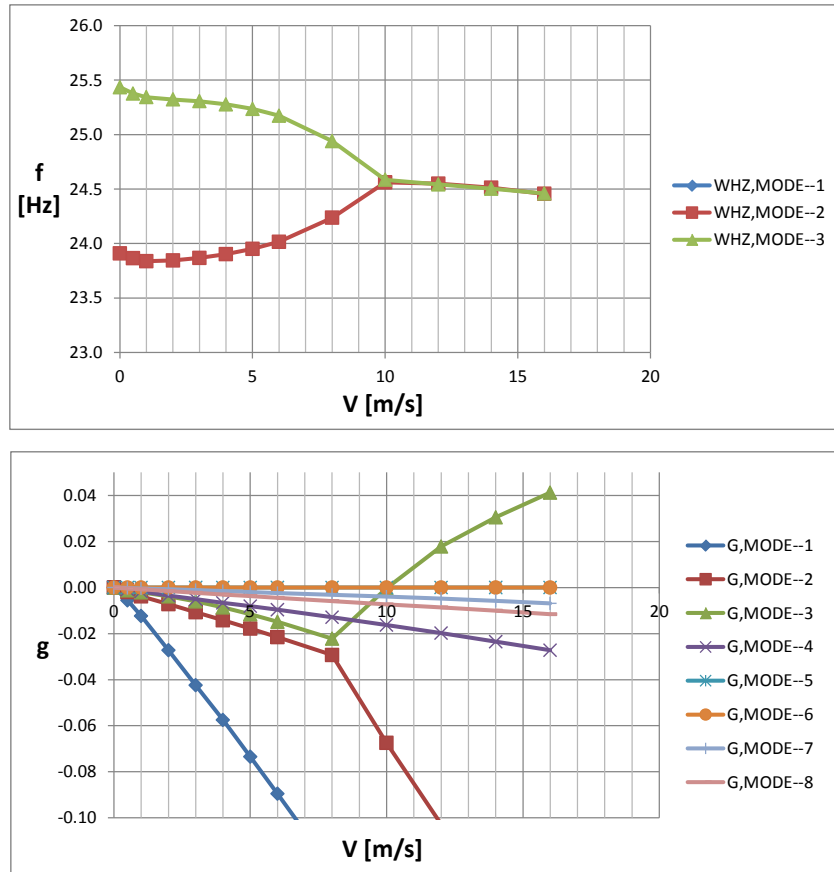


Figure 10: V-g-f curves for flutter investigation - case 5mm neg.

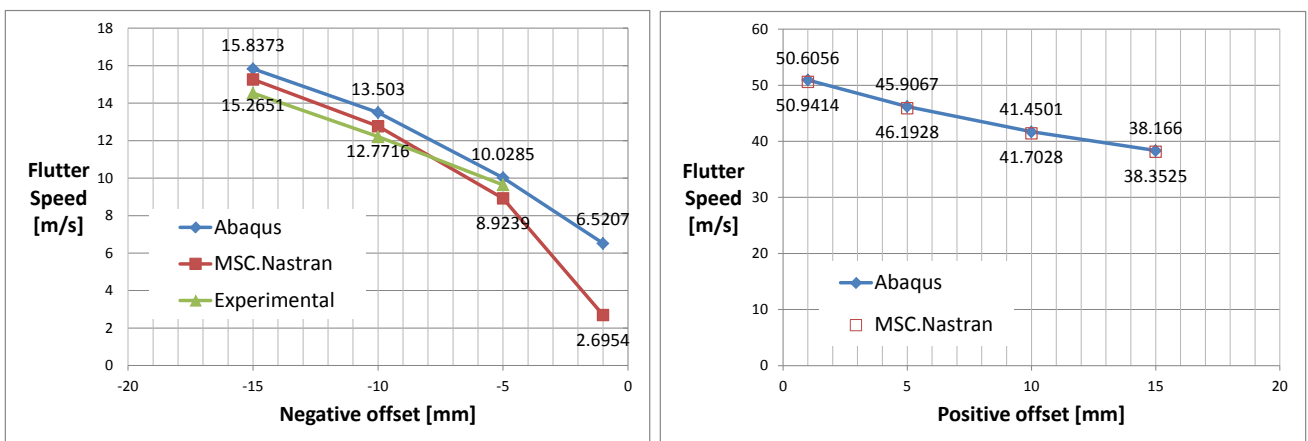


Figure 11: Variation of the flutter velocity with ballast offset positions.

6 ON-GOING AND FUTURE WORKS

Developments are currently on course for the case study of the generic commuter aircraft shown in Figure 5. The aerodynamic discretization is still on-going in order to subsequently implement the same methodology of aeroelastic coupling as was done with the rectangular plate-like wing. Variations of the systems components mass contributions are expected to be performed for parametric analysis and their impact on the aeroelastic characteristics.

On the other hand, a third case study of a micro-gravity sounding rocket at the first stage flight trajectory. Da Silva et al. [10] have studied in detail the flutter mechanism of the VSB-30, a two-stage spinning-stabilized slender sounding rocket with two sets of three fins on each stage, whose engines use a solid propellant. They have concluded that the spinning effect on the ballistic trajectory, used for increasing vehicle flight stability and decreasing vehicle impact point dispersion, does not play a significant role, mainly because the flutter margins remain almost unaltered with and without VSB-30 body spin. It was identified the spinning effect slightly contributes to aeroelastic stability up to a rotation speed to 10 cycles per second. However, rotation effects analyses were limited to centrifugal softening (aparent mass) and stiffening (pre-tension due to centrifugal loads). Current studies are considering gyroscopic damping effects and its influence on the complex mode solution with damping ratios for the aeroelastic dynamic stability via a *COMPLEX FREQUENCY Abaqus procedure with *DLOAD, ROTDYNF load definitions.

7 CONCLUSIONS

Results from the present investigations showed reasonably accurate values for trim, dynamic response and flutter phenomena. Discrepancies between Abaqus and MSC.Nastran manifest when flutter predictions occur at extremely low speed values. Generalizations can be done for more complex aircraft, as in the case of the generic commuter aircraft. In each case a dependence on the aerodynamic mesh size is evident to capture the gradient of pressure distribution and aerodynamic characteristics at near discontinuity regions.

The time simulation process is still in development, since the aerodynamic loading is not yet running inside a user routine of Abaqus. However, the work is following a planned path and the results obtained so far are promising.

ACKNOWLEDGEMENTS

The authors acknowledge the support from the *Instituto Nacional de Ciência e Tecnologia - Estruturas Inteligentes em Engenharia*, INCT-EIE, under Grant No. 674001/2008-5, the *Conselho Nacional de Desenvolvimento Científico e Tecnológico*, CNPq, the *Centro de Pesquisa, Inovação e Difusão do Centro de Ciências Matemáticas Aplicadas à Indústria*, CEPID-CeMEAI and also the *Fundação de Amparo à Pesquisa do Estado de São Paulo*, FAPESP during the course of this work.

REFERENCES

- [1] ZONA Technology Inc., *ZAERO Theoretical Manual 9.0A*, Scottsdale, AZ, USA, 2014.
- [2] Dassault Systèmes SIMULIA Corp., *Abaqus Documentation Collection 6.14*, Providence, RI, USA, 2014.

- [3] Theodorsen T., *NACA-TR-496: General Theory of Aerodynamic Instability and the Mechanism of Flutter*, National Advisory Committee for Aeronautics, USA, 1935.
- [4] Rodden W.P., Johnson E.H., *MSC.NASTRAN Aeroelastic Analysis User's Guide (Version 68)*, MacNeal-Schwendler Corp., USA, 1994.
- [5] Chen P.C., *Damping Perturbation Method for Flutter Solution: The g-Method.*, AIAA Journal, Vol. 38 No. 9, pp. 1519-1524, USA, 2000.
- [6] Westin M.F., et al., *Aeroservoelastic Modeling of a Flexible Wing for Wind Tunnel Flutter Test*, 20th ABCM International Congress of Mechanical Engineering, Gramado, RS, Brazil, 2009.
- [7] Westin M.F., *Aeroelastic Modeling and Experimental Analysis of a Flexible Wing for Wind Tunnel Flutter Test*, Master's Thesis, ITA, Brazil, 2010.
- [8] Kalman T.P., Giesing J.P., Rodden W.P., *Spanwise Distribution of Induced Drag in Subsonic Flow by the Vortex Lattice Method*, AIAA Journal of Aircraft, Vol. 7 No. 6, pp. 574-576, USA, 1970.
- [9] Foltran R.F., *Efeito da Sustentação Estática, Diedro e outros Parâmetros na Determinação das Velocidades de Flutter em Caudas-T*, Master's Thesis, ITA, Brazil, 2010.
- [10] Da Silva R.G.A., et al. *A Sensitivity Investigation on the Aeroelastic Dynamic Stability of Slender Spinning Sounding Rockets*, International Forum on Aeroelasticity and Structural Dynamics, Stockholm, Sweden, 2007.
- [11] Blair W., Williams M., and Weisshaar T., *Time Domain Simulations of a Flexible Wing in Subsonic Compressible Flow*, 31st AIAA Structures, Structural Dynamics and Materials Conference, doi:10.2514/6.1990-1153, Long Beach, CA, USA, 1990.
- [12] Blair M., Williams M. H. *Time Domain Panel Method for Wings*, AIAA Journal of Aircraft, Vol. 30 No. 4, pp. 439–445, doi:10.2514/3.46364, USA, 1993.